https://doi.org/10.5194/egusphere-2025-4415
Preprint. Discussion started: 1 October 2025

Experimental determination of the global warming potential of carbonyl fluoride

Dongkyum Kim[1], Jeongsoon Lee[1,2]

[1]Semiconductor and Display Metrology Group, Korea Research Institute of Standards and Science (KRISS), 267 Gajeong-ro, Yuseong-gu, Daejeon 34113, Republic of Korea
[2]Science of Measurement, University of Science and Technology (UST), 217 Gajeong-ro, Yuseong-gu, Daejeon 34113, Republic of Korea

Correspondence to: Jeongsoon Lee (leejs@kriss.re.kr)

Abstract. Carbonyl fluoride (COF_2) has recently attracted attention as a potential low-global-warming-potential (GWP) replacement for high-GWP fluorinated gases (F-gases) used in semiconductor and display manufacturing, such as HFCs, PFCs, SF_6, and NF_3, because of its proven efficacy as a chamber-cleaning gas and rapid hydrolysis in moist air. In this study, the infrared absorption cross-section (ACS) of COF_2 was measured using Fourier-transform infrared spectroscopy, and its radiative efficiency (RE) was calculated using a revised form of the Pinnock curve that incorporates stratospheric temperature adjustment, yielding 0.1413 $W \cdot m^{-2} \cdot ppb^{-1}$. Atmospheric lifetimes of COF_2 determined from kinetic decay profiles were 7.56 h, 36.67 min, and 54.86 min for dry synthetic air (O_2-only), high-humidity, and low-humidity conditions, respectively, corresponding to GWP_{100} values of 0.1018, 0.0082, and 0.0117, respectively. Accordingly, in moist tropospheric air, COF_2 exhibited $GWP_{100} < 1$. These results demonstrate that water vapor–driven hydrolysis overwhelmingly governs COF_2 removal in the atmosphere, leading to a substantially shorter lifetime and far lower GWP than conventional F-gases. Furthermore, since CO_2 is the confirmed terminal degradation product, the ultimate climate impact of COF_2 is equivalent to that of CO_2 on a molar basis. This study presents one of the most comprehensive experimental analyses of COF_2 and offers a robust evaluation of its GWP and its potential as a sustainable alternative for reducing the climate footprint of semiconductor and display manufacturing processes.

1. Introduction

The growing climate crisis has intensified the global focus on greenhouse gases (GHGs) that drive global warming. While carbon dioxide (CO_2) remains the most prevalent and widely discussed GHG, a range of industrial and synthetic gases

https://doi.org/10.5194/egusphere-2025-4415
Preprint. Discussion started: 1 October 2025

exert disproportionately large climate impacts despite their much smaller quantities due to their high radiative efficiencies and long atmospheric lifetimes (Hodnebrog et al., 2013). To enable meaningful comparisons among these gases, the Intergovernmental Panel on Climate Change (IPCC) introduced the concept of Global Warming Potential (GWP) in its First Assessment Report (IPCC, 1990). GWP quantifies the cumulative radiative forcing (RF) of a greenhouse gas over a specified time horizon relative to the same mass of CO_2. The most commonly used metric GWP_{100} evaluates the climate impact over a 100-year period (Hodnebrog et al., 2020), with CO_2 corresponding to a GWP of 1. In contrast, synthetic gases frequently used in industrial applications, such as nitrogen trifluoride (NF_3) and sulfur hexafluoride (SF_6), have GWP values of 17,200 and 23,500, respectively (NOAA, 2018). These figures underscore the significant warming potential of even trace emissions of such compounds.

GWP is governed by two key parameters (Hodnebrog et al., 2013, 2020; IPCC, 1990, 2021): radiative efficiency (RE), which reflects a gas's ability to absorb infrared radiation, and atmospheric lifetime (τ), which defines a gas's persistence in the atmosphere. The RE ($W \cdot m^{-2} \cdot ppb^{-1}$) of both the target gas (x) and CO_2 quantifies their respective contributions to RF per unit concentration. Atmospheric lifetime influences how long a gas continues to exert warming effects after emission. GWP is calculated using the following equation:

$$GWP_x = \frac{RE_x \cdot \left(\frac{1\,kg}{MW_x}\right) \cdot \int_0^{TH} \exp\left(-{}^{t}/_{\tau_x}\right) dt}{RE_{CO2} \cdot \left(\frac{1\,kg}{MW_{CO2}}\right) \cdot \int_0^{TH} \exp\left(-{}^{t}/_{\tau_{CO2}}\right) dt} \qquad (Equation\ 1)$$

Molecular weight (MW) enables the conversion from molecule count to mass-based emissions, thus ensuring GWP is expressed per kilogram. The integration period for GWP, known as the time horizon (TH), is typically 100 years (GWP_{100}), which is consistent with climate reporting standards. For a more detailed representation, the exponential decay of RF is considered through the following integrals: $\int_0^{TH} \exp\left(-{}^{t}/_{\tau_x}\right) dt$ and $\int_0^{TH} \exp\left(-{}^{t}/_{\tau_{CO2}}\right) dt$. These integrals represent the cumulative atmospheric burden over time (t), accounting for removal processes and persistence.

RE is evaluated based on the gas's infrared absorption cross-section (ACS) together with its spectral overlap with Earth's outgoing infrared radiation (Elrod, 1999; Pinnock et al., 1995), where the ACS defines the probability of photon absorption at specific wavenumbers. RE depends not only on the magnitude of the ACS but also on its alignment with relatively transparent regions of Earth's infrared spectrum (Bera et al., 2010), most notably the atmospheric window (8–14 μm), where radiation escapes to space with minimal absorption and cools the planet. Gases that absorb in spectral windows with minimal overlap with major atmospheric absorbers—such as CO_2, H_2O, CH_4, O_3, and N_2O—contribute more strongly to RF. Wavelength-dependent ACS data are obtained from infrared absorption spectra. The infrared absorption spectrum of GHG can be obtained using a Fourier-transform infrared (FTIR) spectrometer equipped with an optical path gas cell (Harrison, 2015, 2020; Trisna et al., 2023). It is important to distinguish between the measured infrared absorbance and the

https://doi.org/10.5194/egusphere-2025-4415
Preprint. Discussion started: 1 October 2025

ACS. While absorbance reflects the attenuation of infrared light based on the gas concentration and optical path length, as described by the Beer–Lambert law, ACS is a molecular property that quantifies the probability of photon absorption per molecule at each wavenumber. Unlike absorbance, ACS is independent of experimental conditions, such as pressure and concentration, and is typically expressed in units of $cm^2 \cdot molecule^{-1}$.

To derive the infrared ACS of a GHG from FTIR measurements, transmittance spectra are converted using a well-established relation based on the Beer–Lambert law combined with the ideal gas law (Harrison, 2015, 2020). The ACS at a given wavenumber $\tilde{\upsilon}$, denoted as $\sigma(\tilde{\upsilon})$, is calculated using the following equation:

$$\sigma(\tilde{\upsilon}) = \frac{10^4 \cdot \mathrm{T} \cdot k_B \cdot \ln(\frac{1}{T_r(\tilde{\upsilon})})}{P \cdot L} \qquad (Equation\ 2)$$

where T is the absolute temperature in kelvin, k_B is the Boltzmann constant (1.380649×10^{-23} $Pa \cdot m^3 \cdot K^{-1}$), $T_r(\tilde{\upsilon})$ is the measured spectral transmittance, P is the partial pressure of the target gas in pascals, and L is the optical path length in centimeters. The factor 10^4 accounts for the unit conversion to express $\sigma(\tilde{\upsilon})$ in cm^2/molecule. This approach enables the direct determination of ACS spectra from FTIR data by relating molecular-scale absorption behavior to macroscopic spectroscopic observables under defined experimental conditions.

To quantify RE, the ACS is evaluated against the stratospheric-adjusted Pinnock curve (Shine and Myhre, 2020). In this approach, RE is calculated by multiplying the ACS with the curve at each wavenumber and integrating the product over the spectral range (Elrod, 1999; Hodnebrog et al., 2020; Pinnock et al., 1995). RE is computed as follows:

$$\mathrm{RE} = \sum_i \sigma_i F_i \qquad (Equation\ 3)$$

where σ_i is the ACS ($cm^2 \cdot molecule^{-1}$) and F_i is the spectral intensity of the stratospheric-adjusted Pinnock curve at wavenumber i ($W \cdot m^{-2} \cdot cm$). The summation was performed over the range 649–3000 cm^{-1} in 1 cm^{-1} intervals. GWP values were computed using **Equation (1)** based on the RE from **Equation (3)** and experimentally measured atmospheric lifetimes. Reference values for CO_2 include the following: RE = 1.1×10^{-5} $W \cdot m^{-2} \cdot ppb^{-1}$, MW = 44.01 $g \cdot mol^{-1}$, and τ = 150 years. In addition to serving as a comparative metric, GWP functions as a decision-making tool across regulatory, industrial, and policy domains. It enables the aggregation of diverse emissions into CO_2-equivalent (CO_2-eq) units, thereby facilitating unified greenhouse gas inventories, emissions trading systems, and climate mitigation strategies. In high-emission sectors such as semiconductor manufacturing, GWP is widely employed to evaluate and screen low-GWP alternatives, guiding both process optimization and environmental compliance.

GWP plays a pivotal role in the semiconductor and display industries. The continued miniaturization of transistors and increased complexity of chips have intensified the use of fluorinated gases (F-gases), such as CF_4, C_4F_8, and NF_3, for plasma etching (Jung et al., 2024; Kim et al., 2024; Song et al., 2022) and chamber cleaning (An and Hong, 2023; Kai et al., 2024).

https://doi.org/10.5194/egusphere-2025-4415
Preprint. Discussion started: 1 October 2025

These gases are extremely potent and persistent, with GWPs thousands of times greater than that of CO_2 due to their long atmospheric lifetimes and strong infrared absorption. Consequently, they have been targeted under international climate agreements, including the Kyoto Protocol and its Doha Amendment, as well as the Paris Agreement—all of which emphasize the need to reduce emissions of high-GWP substances (UNFCCC, 1997, 2012, 2015).

To mitigate the environmental footprint of semiconductor processes, carbonyl fluoride (COF_2) has recently gained attention as a promising alternative (Jo et al., 2025; Lugani et al., 2024; Mitsui et al., 2004; Park et al., 2025a, 2025b). According to Mitsui et al. (2004)**,** COF_2 is formed as a byproduct during plasma cleaning with C_2F_6/O_2 mixtures and has been experimentally shown to deliver cleaning performance comparable to that of C_2F_6 while reducing global warming emissions by over 95% (Mitsui et al., 2004). Its molecular structure contains fewer fluorine atoms, and its rapid hydrolysis in the presence of moisture suggests a shorter atmospheric lifetime and thus a lower GWP. COF_2 is also non-flammable, non-explosive, and moderately toxic, making it suitable for industrial use under existing safety protocols. Although COF_2 is regarded as a low-GWP candidate due to its chemical reactivity and expected short lifetime, its GWP has yet to be experimentally quantified under controlled laboratory conditions.

Therefore, this study aims to experimentally determine the GWP_{100} of COF_2 by measuring its infrared absorption characteristics and atmospheric lifetime under controlled conditions. The infrared absorption data are used to calculate RE, while the atmospheric lifetime is determined based on the observed decay of COF_2 in the presence of oxidants (Kurylo and Orkin, 2003), such as water vapor and oxygen. By combining these two parameters, we derive a quantitative GWP_{100} value for COF_2. This work provides scientific validation of COF_2's climate impact and supports its potential as a low-GWP alternative to high-GWP fluorinated gases used in semiconductor and display manufacturing.

2. Experimental section

The infrared ACS required for RE calculations was measured using a Nicolet iS50 FTIR spectrometer (Thermo Fisher Scientific, USA) equipped with a 2.4 m multipass gas cell (Pike Technologies). Time-resolved monitoring of COF_2 decay under different oxidizing conditions was performed using an Arcoptix GASEX OEM FTIR spectrometer (Arcoptix S.A., Switzerland), which is a compact and robust module designed for gas-phase spectroscopy. The spectra were collected at one-minute intervals following the introduction of reactive gases. Spectra from both the Nicolet iS50 and Arcoptix GASEX OEM instruments were recorded at a resolution of 0.5 cm^{-1} using Boxcar apodization. During the FTIR measurements, COF_2, the primary sample, was measured within the linear response range. (**Fig. S1** in the Supporting Information, hereafter

https://doi.org/10.5194/egusphere-2025-4415
Preprint. Discussion started: 1 October 2025

SI). An in-house LabVIEW-based control system was implemented to synchronously log temperature and pressure within the gas cell for each spectral acquisition, thereby minimizing operational uncertainty.

The experimental setup and corresponding measurement sequence are shown in **Fig. 1**. In the configuration (**Fig. 1a**), an FTIR spectrometer, MKS 626D Unheated Absolute Baratron® capacitance manometer, PT100 RTD temperature sensor, and Fluke 1586A Super-DAQ Precision Temperature Scanner were integrated into a single system. All components were synchronized and controlled through a LabVIEW-based interface, enabling seamless data acquisition (DAQ) and measurement control. The measurement protocol began with 2.7 s of simultaneous pressure and temperature logging, followed by 10.3 s of FTIR spectral acquisition averaged over 16 scans, as illustrated in **Fig. 1b**. Each cycle concluded with a 57 s idle period before repetition, yielding fully synchronized pressure, temperature, and infrared spectral data at one-minute intervals.

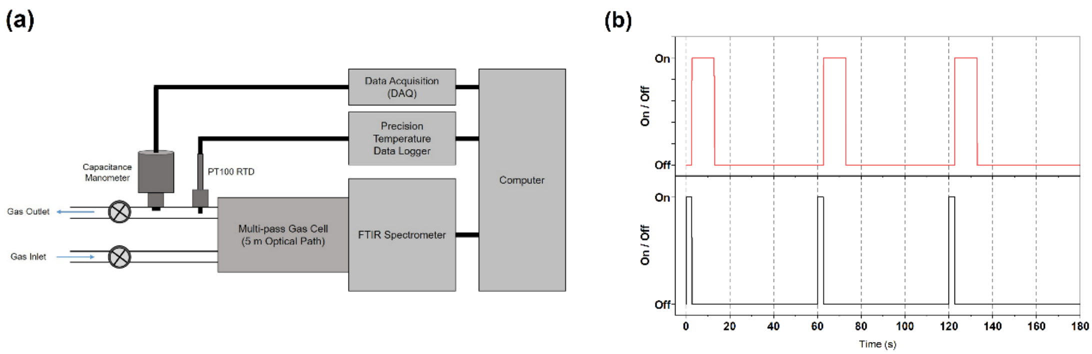

Figure 1. Schematic representation of the experimental system and its measurement sequence. (a) Experimental setup consisting of an FTIR spectrometer, capacitance manometer with data acquisition (DAQ), and PT100 RTD sensor with temperature logging systems, all integrated and controlled via LabVIEW for synchronized measurement control. (b) Time sequence of the measurement cycle: each cycle begins with simultaneous pressure and temperature acquisition for 2.7 s (black solid line), followed by FTIR spectral acquisition for 10.3 s (red solid line, 16 scans averaged). The sequence then includes a 57 s idle period before the next cycle begins, resulting in one complete measurement cycle per minute. This procedure yields synchronized pressure, temperature, and infrared absorption spectra at 1-minute intervals.

Three certified gas mixtures, each contained in high-pressure cylinders, were used in conjunction with humid ambient air drawn from outside the laboratory (**Table 1**). The first cylinder contained COF_2 diluted in nitrogen (COF_2/N_2, 3.360×10^3 µmol mol^{-1}; Sole Materials Co., Ltd., Republic of Korea), which served as the primary sample for infrared measurements and enabled kinetic monitoring of COF_2 decay for atmospheric lifetime determination. The second cylinder held an NF_3/N_2 mixture (2.998×10^2 µmol mol^{-1}), which was gravimetrically prepared and certified by the Korea Research

https://doi.org/10.5194/egusphere-2025-4415
Preprint. Discussion started: 1 October 2025

Institute of Standards and Science (KRISS). Since NF_3 is chemically stable under the experimental conditions, any observed changes in its spectral signature indicated physical leakage rather than chemical reaction. The third cylinder supplied rigorously dehydrated synthetic air (20.9 % O_2 in N_2; Air Liquide Korea Co., Ltd., Republic of Korea), which was used to create a moisture-free oxidizing matrix for isolating the oxygen-initiated degradation pathway of COF_2. Humid ambient air was introduced at atmospheric pressure through a carbon-fiber inlet line fitted with a 2 µm mesh filter, providing a realistic atmospheric matrix containing both O_2 and variable water vapor (approximately 41–45 % relative humidity at 25 °C). This carefully defined gas environment enabled the identification of the primary COF_2 decomposition pathways, which were driven by reactions with oxygen and water vapor. It also allowed for the identification of the dominant atmospheric degradation pathways of COF_2 and the estimation of its expected lifetime under realistic atmospheric conditions.

For the dry synthetic air experiment, the reaction cell was first evacuated to below 10^{-2} Torr and then filled with 8.18 Torr of COF_2/N_2 at 23.6 °C. Subsequently, 746.44 Torr of dehydrated synthetic air (N_2: 79.1 %, O_2: 20.9 %, H_2O < 2 ppm) was introduced to bring the system to atmospheric pressure. In the absence of both water vapor and internal standards, any observed decay of COF_2 was attributed solely to oxygen-initiated reactions. Pressure and temperature remained stable within ±0.1 % over a six-hour period, confirming the integrity of the sealed system.

For the humid air experiment, ambient outdoor air, routed through a carbon-fiber inlet line fitted with a 2 µm mesh filter, was mixed with the COF_2 and NF_3/N_2 gas mixture. Two time-separated fills were performed to assess the influence of daily variations in atmospheric conditions. In the first run (10:30), 15.55 Torr of COF_2 and 40.12 Torr of NF_3/N_2 were combined with 754.19 Torr of ambient air at 25.7 °C and 44.3 % relative humidity. In the second run (20:00), 15.17 Torr of COF_2 and 40.23 Torr of NF_3/N_2 were combined with 753.18 Torr of ambient air at 24.9 °C and 41.8 % relative humidity. The NF_3 signal remained constant throughout, confirming that observed changes in COF_2 were due to chemical degradation rather than system leakage. Ambient outdoor conditions were measured and recorded using a LUTRON MHB-382SD humidity, temperature, and barometric pressure meter.

To evaluate the optimized molecular structure as well as the vibrational and infrared absorption properties of COF_2, density functional theory (DFT) calculations were performed using the B3LYP (Becke, three-parameter, Lee–Yang–Parr) hybrid functional in combination with the 6-31++G(d,p) basis set (Becke, 1993; Frisch et al., 1984; Hariharan and Pople, 1973; Kohn and Sham, 1965). This level of theory is well-suited for accurately predicting optimized geometries and vibrational characteristics associated with infrared absorption (Hodnebrog et al., 2013). The detailed computational methods and optimized molecular structure, including the Z-matrix of the molecular geometry, can be found in the Supporting Information (**SI**).

https://doi.org/10.5194/egusphere-2025-4415
Preprint. Discussion started: 1 October 2025

Table 1. Composition and intended purpose of gas samples.

Sample	Nominal concentration (µmol mol^{-1})	Oxidants / Matrix	H_2O present	Primary use	Supplier
COF_2 / N_2	3360	N_2	No	RE, Lifetime	Sole Materials Co., Ltd.
NF_3 / N_2	299.8	N_2	No	Leak check	KRISS[1]
Synthetic air	209,000	O_2 / N_2	No	O_2-only kinetics	Air Liquide Korea
Ambient air		O_2 / N_2	Yes	Real-air kinetics	Collected outdoors

[1] Korea Research Institute of Standards and Science

3. Results and discussion

3-1. Molecular geometry and predicted reactivity

DFT calculations and Valence Shell Electron Pair Repulsion (VSEPR) theory indicated that COF_2 adopts a nearly trigonal planar geometry at the central carbon atom, although its bond angles deviate significantly from the ideal 120° (**Fig. 2a**). This deviation was associated with the lack of equivalency among the three electron domains. The C=O double bond, with its higher electron density, exerted stronger repulsion than the single bonds, thereby pushing the two C–F bonds closer together. Compared with formaldehyde (COH_2), where the C–H bonds retain moderate electron density near the carbon and maintain significant mutual repulsion (**Fig. S2, SI**), the extreme electronegativity of fluorine strongly withdrew electron density from the C–F bonds toward itself. This withdrawal left the carbon side of the C–F bonds electron-deficient, thereby reducing repulsion between them and allowing the C=O double bond to compress the F–C–F angle to ~108° (**Fig. 2a**). The resulting deviation from ideal sp^2 hybridization produced a quasi-planar geometry that perturbed the orbital overlap, further polarizing the carbon center and enhancing its electrophilicity toward nucleophilic attack. Combined with the strong electron-withdrawing effects of the fluorine substituents and the carbonyl group, this distorted trigonal planar geometry generated a highly polarized electronic environment at the carbon atom. As a result, COF_2 was strongly electrophilic and readily experienced nucleophilic attack, particularly by water, which accounts for its rapid hydrolysis under atmospheric conditions.

https://doi.org/10.5194/egusphere-2025-4415
Preprint. Discussion started: 1 October 2025

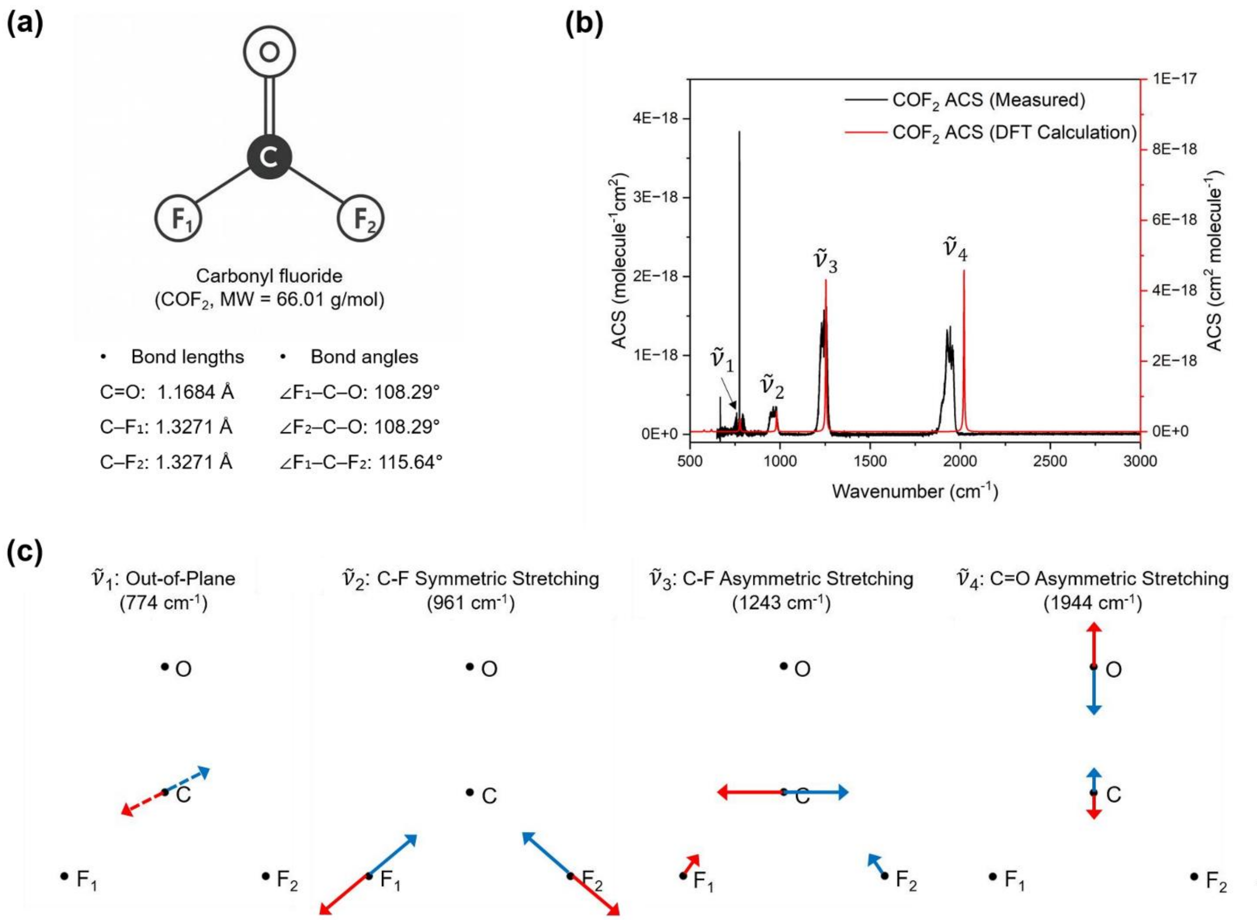

Figure 2. (a) Optimized structure of carbonyl fluoride (COF_2) obtained from DFT calculations. The molecular weight of COF_2 is 66.01 g/mol. The bond lengths are 1.1684 Å for C=O and 1.3271 Å for C–F_1 / C–F_2. The bond angles are ∠F–C–O = 108.29° and ∠F–C–F = 115.39°. These structural parameters indicate that the molecule deviates slightly from planarity. (b) Absorption cross-section (ACS) of COF_2: measured data (black) and DFT-calculated data (red), with labeled vibrational modes ($\tilde{\upsilon}_1$ to $\tilde{\upsilon}_4$). (c) Molecular vibrations corresponding to the labeled modes were as follows: $\tilde{\upsilon}_1$: out-of-plane bending of the carbon atom (774 cm^{-1}), $\tilde{\upsilon}_2$: symmetric C–F stretching (961 cm^{-1}), $\tilde{\upsilon}_3$: asymmetric C–F stretching (1243 cm^{-1}), and $\tilde{\upsilon}_4$: asymmetric C=O stretching (1944 cm^{-1}). The red and blue arrows represent the directions of atomic movement during vibration, with arrows of the same color indicating simultaneous movement, while opposite-colored arrows show movements in opposite directions within the molecule.

https://doi.org/10.5194/egusphere-2025-4415
Preprint. Discussion started: 1 October 2025

3-2. Infrared absorption characteristics and radiative efficiency of COF_2

To evaluate the GWP of COF_2, its infrared absorption characteristics were first examined because they are essential for estimating RE. The infrared transmittance spectrum of COF_2 was recorded using an FTIR spectrometer equipped with a 2.4 m optical-path gas cell. The measured transmittance data were converted to the ACS of COF_2 using the Beer–Lambert law in combination with the ideal gas law, which together relate infrared absorption to molecular number density and optical path length (**Equation (2)**, **Fig. 2b and 3a**). The resulting ACS is an intrinsic molecular property, independent of gas concentration or path length, and is critical for the subsequent calculation of RE and GWP.

As shown in **Fig. 2b-c**, the ACS spectrum of COF_2 exhibited four prominent infrared absorption bands, each of which corresponded to distinct vibrational modes. The strong peak observed near 1944 cm^{-1} ($\tilde{\upsilon}_4$) was attributed to the asymmetric stretching of the C=O bond, where the oxygen atom undergoes significant displacement relative to the central carbon atom. This mode is highly IR-active due to the substantial change in dipole moment along the molecular axis. Another intense feature centered at 1243 cm^{-1} ($\tilde{\upsilon}_3$) corresponded to the asymmetric stretching of the two C–F bonds, where both fluorine atoms vibrate out of phase, enhancing the IR intensity through dipole fluctuation perpendicular to the C=O axis. A third notable band appeared at 961 cm^{-1} ($\tilde{\upsilon}_2$), corresponding to the symmetric stretching of the C–F bonds, in which both fluorine atoms moved simultaneously in phase along the bond axis. Although this mode involves smaller dipole changes than the asymmetric counterpart, it is still IR-active due to the partial asymmetry induced by the overall molecular geometry. Additionally, the ACS spectrum revealed a distinct absorption band at 774 cm^{-1} ($\tilde{\upsilon}_1$) that corresponded to the out-of-plane bending (or wagging) motion of the carbon atom relative to the quasi-planar F–C–O framework. This low-energy mode provides information on vibrational motions that deviate from the molecular plane and contributes to the characteristic vibrational fingerprint of COF_2. The correspondence between these vibrational modes and the ACS peaks confirms their vibrational origins and demonstrates the ability of the quantum mechanical simulations to reproduce experimentally observed spectral features.

Based on this spectrum, RE was calculated according to the stratospheric-adjusted Pinnock curve (Shine & Myhre, 2020), which integrates the product of the wavenumber-dependent ACS and the stratospheric-adjusted Pinnock curve. The stratospheric-adjusted Pinnock curve is shown in **Fig. 3a** as a red line, representing Earth's thermal emission profile. The overlap between the COF_2 ACS (black line) and stratospheric-adjusted Pinnock curve highlights the spectral regions that contribute most significantly to infrared absorption. To quantify this interaction, the pointwise product of the ACS and stratospheric-adjusted Pinnock curve was computed to yield the spectral RE contribution, which is plotted in **Fig. 3b** (solid black line). The RE spectrum shows that dominant contributions primarily corresponded to the 750–1300 cm^{-1} region, where both molecular absorption and Earth's emission intensity are strong. The cumulative RE curve (dotted line in **Fig.**

https://doi.org/10.5194/egusphere-2025-4415
Preprint. Discussion started: 1 October 2025

3b) increased steeply in this range and leveled off beyond ~1300 cm⁻¹, indicating that most of COF_2's RF is concentrated within this mid-infrared band. A small step-like increase was also observed near 1900 cm⁻¹, where COF_2 exhibits a strong ACS. However, the corresponding stratospheric-adjusted Pinnock curve in this region was minimal, leading to only a minor contribution to the total RE. Integrating over the full wavenumber range (**Equation (3)** and **Fig. 3b**) yields a total per-molecule RE of 0.1413 W m^{-2} ppb^{-1}. Although lower than that of many fully fluorinated compounds, COF_2's spectral alignment with the stratospheric-adjusted Pinnock curve regions confirms a measurable contribution to RF.

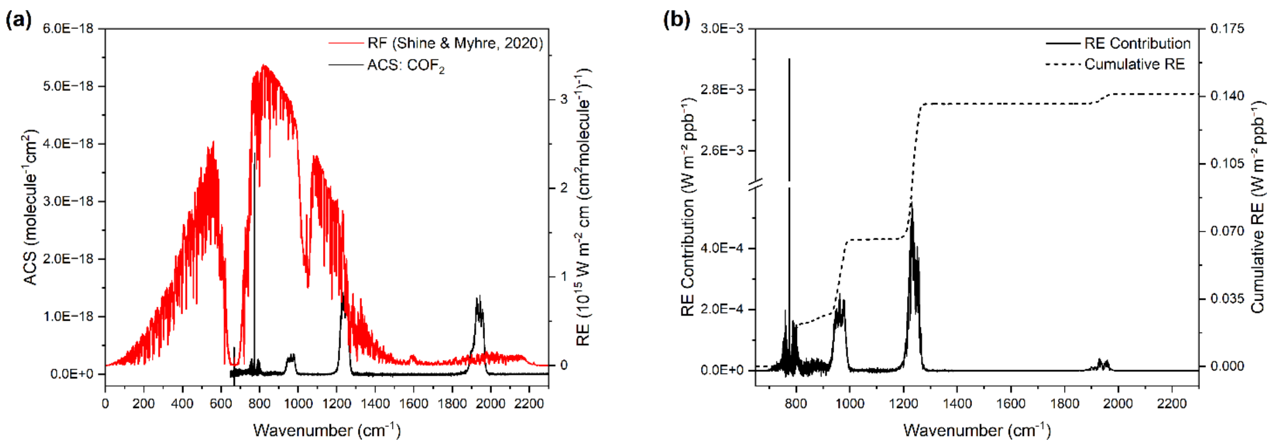

Figure 3. Radiative efficiency (RE) calculation framework for carbonyl fluoride (COF_2) based on its infrared absorption characteristics and the stratospheric-adjusted Pinnock curve. (a) Infrared absorption cross-section (ACS) spectrum of COF_2 overlaid with the Earth's emission spectrum derived from the stratospheric-adjusted Pinnock curve (Shine & Myhre, 2020). The ACS of COF_2 was constructed by regionally combining two spectra acquired at different concentrations and stitching them at 1998.803 cm⁻¹ to produce a single ACS spectrum. High-concentration (170.65 Torr / 296.79 K) data were used in weakly absorbing regions to improve SNR, and low-concentration (40.24 Torr / 296.77 K) data were used in strongly absorbing regions to avoid saturation, consistent with the concentration-independence of ACS. (b) RE contribution spectrum calculated as the product of the ACS and the terrestrial emission spectrum, as described by Equation (3). The cumulative RE, obtained by integrating the RE contribution across the wavenumber range, reaches a final value of 0.1413 W·m⁻²·ppb⁻¹. This figure represents both the methodology and outcome of the RE calculation approach.

3-3. Comparative kinetic assessment of O_2- and H_2O-mediated COF_2 degradation

Understanding the atmospheric removal mechanisms of COF_2 is essential for accurately estimating its atmospheric lifetime and global warming potential. In the troposphere, COF_2 can be removed via oxidation by molecular oxygen (O_2) and hydrolysis by water vapor (H_2O), with the latter generally expected to dominate under humid conditions. To distinguish

https://doi.org/10.5194/egusphere-2025-4415
Preprint. Discussion started: 1 October 2025

between these pathways, experiments were conducted under two contrasting atmospheric conditions: (i) a dried synthetic air mixture containing O_2 but negligible H_2O (< 2 ppm) and (ii) ambient outdoor air containing O_2 along with typical atmospheric water vapor concentrations. The dried synthetic air experiments provided a reference kinetic profile for O_2-only oxidation, whereas the humid air experiments quantified the enhancement in COF_2 loss attributable to hydrolysis.

Scheme 1. Proposed atmospheric removal pathways of COF_2.

(a) O_2-initiated oxidation (dry oxidation matrix):

$$COF_2(g) + O_2(g) \rightarrow CO_2(g) + \text{F-bearing oxidized products}$$

(b) Hydrolysis (dominant in humid air):

$$COF_2(g) + H_2O(g) \rightarrow CO_2(g) + 2HF(g)$$

The primary objective of the $COF_2 + O_2$ experiments in dried synthetic air was to establish a baseline reaction profile under controlled, water-free conditions. This approach isolates the oxidative pathway involving O_2, enabling direct comparison with real atmospheric mixtures containing multiple reactive species. The time-resolved FTIR spectra (**Fig. 4a**) showed the progressive decay of COF_2 absorption bands alongside the concurrent growth of CO_2 features during oxidation. Integrated absorbance profiles for the COF_2 bands (Band 1: 931–998 cm^{-1}; Band 2: 1167–1311 cm^{-1}; Band 3: 1854–2004 cm^{-1}) followed exponential decay trends (**Fig. 4b**), while the CO_2 band (Band 4: 2284–2391 cm^{-1}) exhibited exponential growth (**Fig. 4c**). The fitted time constants (τ), summarized in **Table 2**, yielded average values of 453.66 min for COF_2 decay and 590.79 min for CO_2 production, indicating a direct kinetic linkage between the two processes. These results correspond to an atmospheric lifetime of approximately 7–8 h for COF_2 under dry synthetic air conditions, where the dominant oxidative pathway is reaction with O_2 and the principal product is CO_2. The slight difference between the decay rate of COF_2 and the growth rate of CO_2 suggests the formation of intermediate species during the COF_2–O_2 reaction. However, the quantity of such intermediates is likely below the detection limit of the FTIR spectrometer used, reflecting both their low abundance and inherent instability. These O_2-only kinetics provide a baseline reference for assessing the role of water vapor in subsequent experiments.

https://doi.org/10.5194/egusphere-2025-4415
Preprint. Discussion started: 1 October 2025

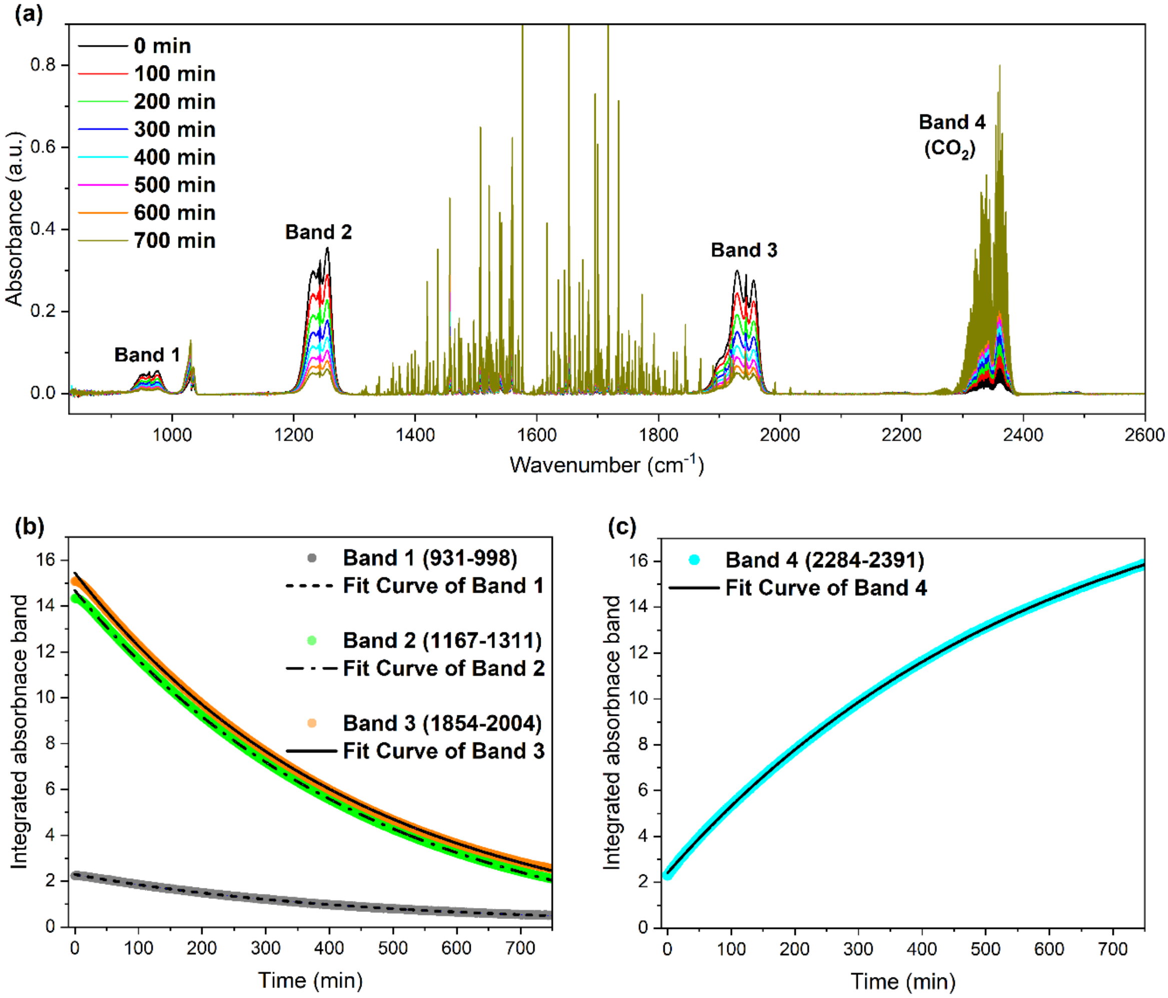

Figure 4. Infrared spectroscopic analysis of the reaction between carbonyl fluoride (COF_2) and molecular oxygen (O_2), showing both the depletion of COF_2 and the formation of CO_2 over time. (a) Time-resolved infrared absorbance spectra of COF_2 during its reaction with O_2, showing the gradual decay of COF_2 and concurrent increase in CO_2 absorption features. Spectra were recorded at 100-minute intervals up to 700 minutes. (b) Integrated absorbance of COF_2 bands (Band 1: 931–998 cm^{-1}, Band 2: 1167–1311 cm^{-1}, Band 3: 1854–2004 cm^{-1}) as a function of time, illustrating the exponential decay of COF_2. (c) Integrated absorbance of the CO_2 band (Band 4: 2284–2391 cm^{-1}), indicating the formation and accumulation of CO_2 over time.

Table 2. Exponential fitting parameters for the decay of COF_2 or increase of CO_2 under various atmospheric conditions. Each entry corresponds to a specific vibrational band, with parameters obtained from fitting the time-resolved data to the

https://doi.org/10.5194/egusphere-2025-4415
Preprint. Discussion started: 1 October 2025

function $\mathbf{y} = \boldsymbol{A}\boldsymbol{e}^{-x/\tau} + \boldsymbol{C}$. COF_2–Ambient Air (Morning)" and "COF_2–Ambient Air (Afternoon)" indicate experiments conducted during different times of the day to reflect ambient variation. The time constant (τ) represents the characteristic time of the exponential process, and the average τ was calculated across all bands within each sample type.

Sample Type	Kinetic Process / Spectral Band	Amplitude (A)	Time Constant (τ, s)	Offset (C)	Average τ (s)
COF2-O2	COF2 Decay: Band 1	2.206	442.442	0.088	453.662
	COF2 Decay: Band 2	15.832	467.844	-1.149	
	COF2 Decay: Band 3	16.024	450.699	-0.577	
	CO2 Rise: Band 4	-18.715	-590.787	21.122	590.787
COF2-Ambient Air (Morning)	COF2 Decay: Band 1	3.065	34.817	-0.333	36.674
	COF2 Decay: Band 2	23.065	37.850	-0.181	
	COF2 Decay: Band 3	25.003	37.355	6.202	
COF2-Ambient Air (Afternoon)	COF2 Decay: Band 1	3.209	52.272	-0.490	54.862
	COF2 Decay: Band 2	23.462	56.744	-0.463	
	COF2 Decay: Band 3	25.425	55.570	5.390	

The ambient air experiments were designed to evaluate COF_2 removal under realistic atmospheric conditions and quantify the relative contribution of hydrolysis. Ambient air contains, in addition to oxygen and nitrogen, water vapor, argon, and other trace-level gases. The sampling location did not have any unusual atmospheric characteristics; therefore, the air composition is considered representative of typical outdoor conditions. Two time-separated fills were performed to assess the effect of daily variations in atmospheric parameters. Morning (10:30) and evening (20:00) trials on the same day leveraged differences in relative humidity to probe the sensitivity of COF_2 degradation to the water vapor content. Comparative results (**Fig. 5**) showed that COF_2 decays significantly faster under higher humidity in the morning (**Fig. 5a,b**) than under the lower humidity in the evening (**Fig. 5c,d**). As summarized in **Table 2**, the average τ in the morning (36.67 min) was markedly shorter than that in the evening (54.86 min). This accelerated removal in humid air was consistent with the hydrolysis pathway, in which H_2O reacted with COF_2 more rapidly and dominantly than O_2. NF_3 was introduced into

https://doi.org/10.5194/egusphere-2025-4415
Preprint. Discussion started: 1 October 2025

the reaction cell as an inert indicator gas to verify system airtightness. No change was observed in the NF_3 absorption bands during the experiments (**Fig. 5a,c**), confirming that the reaction cell remained sealed with no exchange of gases with the external environment.

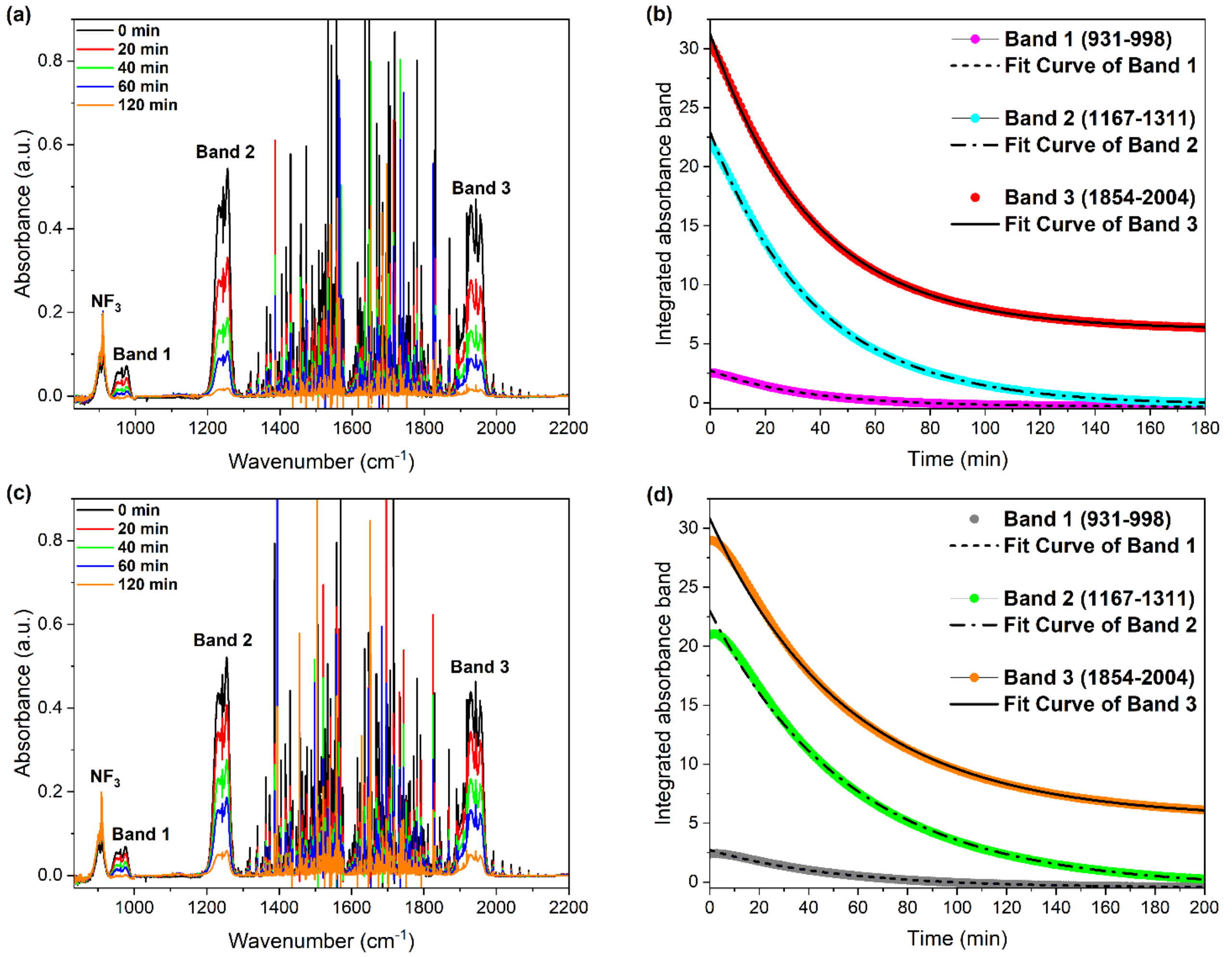

Figure 5. Atmospheric degradation behavior of COF_2 under ambient air conditions, illustrating the influence of atmospheric moisture on the reaction kinetics. (a, b) Spectral and kinetic analysis of COF_2 decay measured in the morning, when the relative humidity was higher. (a) Time-resolved FTIR absorbance spectra showing the decay of COF_2 features. (b) Integrated absorbance of three representative COF_2 bands (Band 1: 931–998 cm^{-1}, Band 2: 1167–1311 cm^{-1}, Band 3: 1854–2004 cm^{-1}) and corresponding exponential decay fits. (c, d) Measurements taken in the afternoon under relatively lower humidity conditions. (c) Time-resolved spectra showing slower spectral decay. (d) Kinetic profiles of the same COF_2 bands as in (b) but highlighting the slower decay under drier atmospheric conditions. These results confirm that the presence of higher ambient moisture accelerates the degradation of COF_2 in air. To clearly display each spectrum, Figures (a) and (c) were plotted after

subtracting the water vapor spectra obtained after the reaction was completed under the morning conditions (a) and the afternoon conditions (c). For details, see SI (Figures S3–S4).

Direct comparisons between the O_2-only and ambient air experiments confirmed the experimental objective of separating and quantifying the roles of major atmospheric oxidants in COF_2 degradation. The results clearly indicate that hydrolysis with H_2O proceeded faster and was more dominant than oxidation by O_2. In the actual atmosphere, OH radicals—another potential oxidant—were present at concentrations of ~10^6 molecules cm^{-3} during daylight hours, although these levels were still several orders of magnitude lower than those of water vapor or oxygen (Seinfeld and Pandis, 2006). Furthermore, the reactivity of COF_2 toward H_2O and O_2, combined with their much higher atmospheric abundances, rendered the OH pathway negligible in comparison. Therefore, hydrolysis overwhelmingly governed the atmospheric removal rate of COF_2, with O_2 oxidation playing a secondary role.

3-4. GWP_{100} of COF_2 under dry and humid atmospheric conditions

Table 3 summarizes the environmental parameters, atmospheric lifetimes, radiative efficiencies, and GWP_{100} values measured under dry air and ambient air conditions. The RE of COF_2, calculated from its ACS spectrum using the stratospheric-adjusted RF efficiency (Shine & Myhre, 2020), was 0.1413 $W \cdot m^{-2} \cdot ppb^{-1}$ on a per-molecule basis. In dry synthetic air, COF_2 exhibited an atmospheric lifetime of approximately 7.56 h (τ = 453.66 min), and when combined with the RE, it yielded a GWP_{100} value of 0.1018. Under humid ambient air conditions, the lifetime was reduced to 36.67 min in the morning (high humidity) and 54.86 min in the evening (low humidity). These shorter lifetimes corresponded to much lower GWP_{100} values of 0.0082 (morning) and 0.0117 (afternoon). This comparison clearly showed that the substantially shorter lifetime of COF_2 in humid air directly translated to significantly reduced GWP values compared to that under dry air conditions. Even when considering only the reactions with the major atmospheric constituents O_2 and H_2O, the GWP_{100} of COF_2 was markedly lower than that of other fluorinated compounds typically classified as greenhouse gases. Furthermore, since CO_2 was the confirmed terminal atmospheric degradation product of COF_2, its ultimate climate impact was equivalent to that of CO_2 itself.

Table 3. Environmental conditions and resulting radiative efficiency, atmospheric lifetime, and 100-year global warming potential (GWP_{100}) for COF_2 measured under ambient air. Humidity and temperature were measured simultaneously with FTIR spectroscopic observations, and the lifetime corresponds to the exponential decay of COF_2. Radiative efficiency and atmospheric lifetime values were used to compute GWP_{100} according to the IPCC methodology.

https://doi.org/10.5194/egusphere-2025-4415
Preprint. Discussion started: 1 October 2025

Sample Types	Relative Humidity (%)	Temperature (°C)	Absolute Humidity (g/m³)	Chemicals	Radiative Efficiency ($W \cdot m^{-2} \cdot ppb^{-1}$)	Atmospheric Lifetime (min)	GWP_{100}
Dry Synthetic Air	< 0.0068[1)]	23.9	< 0.00147[1)]	COF_2	0.1413	453.662	0.1018
High-Humidity Air (Morning)	44.3	25.7	10.6	COF_2	0.1413	36.674	0.0082
Low-Humidity Air (Afternoon)	41.8	24.9	9.6	COF_2	0.1413	54.862	0.0117

1) Both "< 0.0068" and "< 0.00147" are values calculated from 2 ppm through unit conversion.

4. Conclusion

This study presents an integrated experimental and computational evaluation of the infrared absorption properties, atmospheric reactivity, and climate impact of COF_2. Quantum chemical calculations confirmed that COF_2 possesses a quasi-planar geometry with strong electrophilic character, making it susceptible to rapid hydrolysis in the presence of water vapor. FTIR measurements provided a well-resolved absorption cross-section spectrum, and the vibrational modes associated with the observed absorption bands were analyzed, offering further insights into the infrared-active modes of COF_2. The corresponding RE of 0.1413 $W \cdot m^{-2} \cdot ppb^{-1}$ was determined using the stratospheric-adjusted Pinnock curve. This value quantifies the capacity of COF_2 to trap infrared radiation in the atmosphere.

Kinetic experiments under controlled dry air (O_2-only) conditions and realistic humid air environments revealed that atmospheric water vapor overwhelmingly dominates COF_2 removal via hydrolysis, while oxidation by O_2 plays a secondary role. The measured atmospheric lifetime in dry synthetic air was approximately 7.56 h, whereas that under high humidity and low humidity and ambient air conditions was 36.67 min and 54.86 min, respectively. These substantial differences in lifetime directly translate into large variations in the calculated GWP_{100}: 0.1018 in dry air versus 0.0082 and 0.0117 under high- and low-humidity conditions, respectively. Consequently, under water-vapor–containing tropospheric conditions, COF_2 exhibited $GWP_{100} < 1$.

Even considering only reactions with O_2 and H_2O, the GWP_{100} of COF_2 was markedly lower than that of most greenhouse-classified fluorinated compounds. Moreover, because CO_2 is the confirmed terminal atmospheric degradation product, the ultimate climate impact of COF_2 emissions was effectively equivalent to the release of an equal molar quantity of CO_2. These findings demonstrate that despite its measurable RE, the rapid hydrolytic removal of COF_2 under typical tropospheric conditions severely limits its long-term climate forcing potential. This work provides a critical basis for incorporating realistic atmospheric lifetimes into climate models and for evaluating COF_2 within environmental risk assessments related to industrial emissions.

Data availability

Data are available at Zenodo at https://doi.org/10.5281/zenodo.17119680.

Author contributions

DK conceived and led the topic; designed the experimental strategy; developed the FTIR instrumentation and a measurement workflow tailored to GWP determination; performed measurements and formal analysis; and wrote the original draft. JL, as a project leader, of co-conceived the project and experimental design; supervised the research as principal investigator; contributed to data interpretation; and reviewed and edited the manuscript. Both authors discussed the results and approved the final manuscript.

Competing interests

The authors declare that they have no conflict of interest.

Acknowledgements

We gratefully acknowledge Sole Materials Co., Ltd. (Republic of Korea) for supplying the COF_2-in-nitrogen (COF_2/N_2) gas mixture used in this study, and we especially thank Hyeonki Park (Sole Materials Co., Ltd.) for coordination and technical assistance.

Financial support

This work was supported by the Technology Innovation Program (RS-2022-00155753, "GWP 1,000 or Less Chamber Cleaning Gas and its Remote Plasma System for Low GWP Gas"; RS-2023-00262743, "Development of GWP 150 or lower alternative gas and process technology for chemical vapor deposition chamber cleaning process for display TFT gate insulator film") funded by the Ministry of Trade, Industry and Energy (MOTIE, Korea).

References

https://doi.org/10.5194/egusphere-2025-4415
Preprint. Discussion started: 1 October 2025

An, S. and Hong, S. J.: Spectroscopic Analysis of NF3 Plasmas with Oxygen Additive for PECVD Chamber Cleaning, Coatings, 13, 91, https://doi.org/10.3390/coatings13010091, 2023.

Becke, A. D.: Density-functional thermochemistry. III. The role of exact exchange, J. Chem. Phys., 98, 5648–5652, https://doi.org/10.1063/1.464913, 1993.

Bera, P. P., Francisco, J. S., and Lee, T. J.: Design strategies to minimize the radiative efficiency of global warming molecules, Proc. Natl. Acad. Sci., 107, 9049–9054, https://doi.org/10.1073/pnas.0913590107, 2010.

Elrod, M. J.: Greenhouse Warming Potentials from the Infrared Spectroscopy of Atmospheric Gases, J. Chem. Educ., 76, 1702, https://doi.org/10.1021/ed076p1702, 1999.

Frisch, M. J., Pople, J. A., and Binkley, J. S.: Self-consistent molecular orbital methods 25. Supplementary functions for Gaussian basis sets, J. Chem. Phys., 80, 3265–3269, https://doi.org/10.1063/1.447079, 1984.

Hariharan, P. C. and Pople, J. A.: The influence of polarization functions on molecular orbital hydrogenation energies, Theor. Chem. Acc., 28, 213–222, https://doi.org/10.1007/BF00533485, 1973.

Harrison, J. J.: Infrared absorption cross sections for 1,1,1,2-tetrafluoroethane, J. Quant. Spectrosc. Radiat. Transf., 151, 210–216, https://doi.org/10.1016/j.jqsrt.2014.09.023, 2015.

Harrison, J. J.: New infrared absorption cross sections for the infrared limb sounding of sulfur hexafluoride (SF6), J. Quant. Spectrosc. Radiat. Transf., 254, 107202, https://doi.org/10.1016/j.jqsrt.2020.107202, 2020.

Hodnebrog, Ø., Aamaas, B., Fuglestvedt, J. S., Marston, G., Myhre, G., Nielsen, C. J., Sandstad, M., Shine, K. P., and Wallington, T. J.: Updated Global Warming Potentials and Radiative Efficiencies of Halocarbons and Other Weak Atmospheric Absorbers, Rev. Geophys., 58, e2019RG000691, https://doi.org/10.1029/2019RG000691, 2020.

Hodnebrog, Ø., Etminan, M., Fuglestvedt, J. S., Marston, G., Myhre, G., Nielsen, C. J., Shine, K. P., and Wallington, T. J.: Global warming potentials and radiative efficiencies of halocarbons and related compounds: A comprehensive review, Rev. Geophys., 51, 300–378, https://doi.org/10.1002/rog.20013, 2013.

Intergovernmental Panel on Climate Change (IPCC): Climate Change 2021: The Physical Science Basis. Contribution of Working Group I to the Sixth Assessment Report of the Intergovernmental Panel on Climate Change, edited by: Masson-Delmotte, V., Zhai, P., Pirani, A., Connors, S. L., et al., Cambridge University Press, Cambridge, UK and New York, NY, USA, 2021.

Intergovernmental Panel on Climate Change (IPCC): Climate Change: The IPCC Scientific Assessment, edited by: Houghton, J. T., Jenkins, G. J., and Ephraums, J. J., Cambridge University Press, Cambridge, UK and New York, NY, USA, 1990.

Jo, S. Y., Park, A. H., and Hong, S. J.: Effects of the Applied Power of Remote Plasma System With Green Alternative Chamber Cleaning Gas of Carbonyl Fluoride, IEEE Trans. Semicond. Manuf., 38, 624–633, https://doi.org/10.1109/TSM.2025.3572285, 2025.

Jung, J., Kim, J.-H., Lim, C.-M., Choi, J.-E., Bae, J., Kim, H.-D., and Chung, C.-W.: Low-damage etching of poly-Si and SiO2 via a low-energy electron beam in inductively coupled CF4 plasma, Plasma Sources Sci. Technol., 33, 105013, https://doi.org/10.1088/1361-6595/ad8217, 2024.

Kai, T., Yuang, K., Chou, C., Chuah, K., Peng, L., and Jun, X.: TEOS Integrated High-Low Pressure RPS Clean: APC: Advanced Process Control, 1 pp., https://doi.org/10.1109/ASMC61125.2024.10545361, 2024.

Kim, G., Kwon, J.-W., Lee, I., Seo, H., Park, J.-B., Shin, J.-H., and Kim, G.-H.: Application of Plasma Information-Based Virtual Metrology (PI-VM) for Etching in $C_4F_8/Ar/O_2$ Plasma, IEEE Trans. Semicond. Manuf., 37, 602–614, https://doi.org/10.1109/TSM.2024.3447074, 2024.

Kohn, W. and Sham, L. J.: Self-Consistent Equations Including Exchange and Correlation Effects, Phys. Rev., 140, A1133–A1138, https://doi.org/10.1103/PhysRev.140.A1133, 1965.

Kurylo, M. J. and Orkin, V. L.: Determination of atmospheric lifetimes via the measurement of OH radical kinetics, Chem. Rev., 103, 5049–5076, https://doi.org/10.1021/cr020524c, 2003.

https://doi.org/10.5194/egusphere-2025-4415
Preprint. Discussion started: 1 October 2025

Lugani, G. S., Skaggs, R., Morris, B., Tolman, T., Tervo, D., Uhlenbrock, S., Hacker, J., Seng, C. Tan, Nehlsen, J. P., Ridgeway, R. G., Wong, L. Broadway, and Rudy, F. P.: Direct Emissions Reduction in Plasma Dry Etching Using Alternate Chemistries: Opportunities, Challenges, and Need for Collaboration, IEEE Trans. Semicond. Manuf., 37, 445–452, https://doi.org/10.1109/TSM.2024.3444465, 2024.

Mitsui, Y., Ohira, Y., Yonemura, T., Takaichi, T., Sekiya, A., and Beppu, T.: The Possibility of Carbonyl Fluoride as a New CVD Chamber Cleaning Gas, J. Electrochem. Soc., 151, G297, https://doi.org/10.1149/1.1669010, 2004.

National Oceanic and Atmospheric Administration (NOAA), Burkholder, J. B., Ø. Hodnebrog, and Orkin, V. L., "Appendix A Summary of Abundances, Lifetimes, Ozone Depletion Potentials (ODPs), Radiative Efficiencies (REs), Global Warming Potentials (GWPs), and Global Temperature Change Potentials (GTPs)," [Online] Available: https://csl.noaa.gov/assessments/ozone/2018/downloads/AppendixA_2018OzoneAssessment.pdf, 2018.

Park, A. H., Byun, H., and Hong, S. J.: High-power remote plasma source with alternative gas COF2 for PECVD chamber dry cleaning, Jpn. J. Appl. Phys., 64, 04SP23, https://doi.org/10.35848/1347-4065/adc1d6, 2025.

Park, A. H., Lee, Y., Jo, S., and Hong, S. J.: An Alternative PECVD Chamber Cleaning Gas of COF2 for Low-GWP Consideration, IEEE Trans. Semicond. Manuf., 38, 596–604, https://doi.org/10.1109/TSM.2025.3559471, 2025.

Pinnock, S., Hurley, M. D., Shine, K. P., Wallington, T. J., and Smyth, T. J.: Radiative forcing of climate by hydrochlorofluorocarbons and hydrofluorocarbons, J. Geophys. Res.-Atmos., 100, 23227–23238, https://doi.org/10.1029/95JD02323, 1995.

Seinfeld, J. H. and Pandis, S. N.: Chemistry of the troposphere, in: Atmospheric Chemistry and Physics: From Air Pollution to Climate Change, 2nd Edn., John Wiley & Sons, Hoboken, NJ, USA, pp. 204–279, 2006.

Shine, K. P. and Myhre, G.: The Spectral Nature of Stratospheric Temperature Adjustment and its Application to Halocarbon Radiative Forcing, J. Adv. Model. Earth Syst., 12, e2019MS001951, https://doi.org/10.1029/2019MS001951, 2020.

https://doi.org/10.5194/egusphere-2025-4415
Preprint. Discussion started: 1 October 2025

Song, W. S., Kang, J. E., and Hong, S. J.: Spectroscopic Analysis of CF4/O2 Plasma Mixed with N2 for Si3N4 Dry Etching, Coatings, 12, 64, https://doi.org/10.3390/coatings12081064, 2022.

Trisna, B. A., Park, S., Park, I., Lee, J., and Lim, J. S.: Measurement report: Radiative efficiencies of (CF3)2CFCN, CF3OCFCF2, and CF3OCF2CF3, Atmos Chem Phys, 23, 4489–4500, https://doi.org/10.5194/acp-23-4489-2023, 2023.

United Nations Framework Convention on Climate Change (UNFCCC), "Kyoto Protocol to the United Nations Framework Convention on Climate Change." [Online]. Available: https://unfccc.int/kyoto_protocol(last access: 7 September 2025), 1997.

United Nations Framework Convention on Climate Change (UNFCCC), "Doha Amendment to the Kyoto Protocol." [Online] Available: https://unfccc.int/process/the-kyoto-protocol/doha-amendment(last access: 7 September 2025), 2012.

United Nations Framework Convention on Climate Change (UNFCCC), "Paris Agreement." [Online] Available: https://unfccc.int/process-and-meetings/the-paris-agreement/the-paris-agreement, 2015.